Mon. Not. R. Astron. Soc. **000**, 000–000 (0000) Printed 2 July 2014 (MN LATEX style file v2.2)

Dark Matter Distribution in Dwarf Spheroidals

P. Steger[1⋆], A. Boley[2], J. I. Read[1,3]
[1] *Department of Physics, ETH Zürich, CH-8093 Zürich, Switzerland*
[2] *Department of Astronomy; University of Florida, 211 Bryant Space Science Center, Gainesville, FL 32611, USA*
[3] *Department of Physics, University of Surrey, Guildford, GU2 7XH, UK*

2 July 2014

ABSTRACT
I present results on dark matter distribution in dwarf galaxies found in simulations of representative patches down to redshift 10. The influence of baryons on the dark matter profiles is investigated. Effects from mismatching halo centers are eliminated by applying different halo finder techniques and refinements.

Substructures in the stellar components indicate that several star clusters formed independently before accreting on the center of a halo.

The computed dark matter density profiles can be compared with observations, allowing us to check the underlying cosmological model. With known typical distribution, direct detection dark matter searches can be focused on the densest areas, allowing us to optimize for a higher annihilation detection rate.

Key words: cosmology: theory, large-scale structure of Universe – galaxies: dwarf spheroidals, evolution – methods: numerical

1 INTRODUCTION

What is Dark Matter? Where is it? How does it influence the buildup of structures like the Milky Way?

1.1 General Background

An introduction to dynamics of bound systems is given in e.g. Binney & Tremaine (2008), with emphasis on galaxies. **(TODO: some general concepts)**

1.1.1 Cosmological Models

The cosmological model assumed in this work is based on the ΛCDM model (Weinberg (2008), Peacock (1999)), which basically assumes that there is a varying amount of radiation, baryonic matter, dark matter, and dark energy to fill up the energy density of the Universe. The cosmology uses the 5-year WMAP values (Komatsu et al. 2009) for the cosmological parameters. **(TODO: more info: really used 7-year WMAP values for generation of the ICs? find reference!)**

1.1.2 Structure Formation

Structure is believed to form sequentially on small scales and to contract to oblate structures (sheets), which meet in filaments, along which the material accretes onto big clusters in the intersections. This generates a structure called the Cosmic Web. A more detailed review structure formation through the history of the Universe is found in Padmanabhan (1993).

1.2 Dark Matter

The current measurements (Komatsu et al. 2009) **(TODO: WMAP7 update)** indicate that 83% of the matter density is not interacting with baryonic matter except through gravity and not emitting light, therefore called dark matter.

1.2.1 Evidence for Dark Matter

Several objects in gravitationally bound systems were found to move faster than the escape velocity determined by the potential of the luminous parts. The investigation of high velocities of galaxies in clusters e.g. led Zwicky (1933) to assume the existence of a hitherto unknown, not emitting material called DARK MATTER. Furthermore, galactic rotation curves should show $v(r) \propto \sqrt{M(r)/r}$, with $v(r) \propto r^{-1/2}$ outside the observed, luminous part; instead in most galaxies it rises to a maximum value and stays approximately constant out to the edges of the galaxy. This implies $M(r) \propto r$ or $\rho(r) \propto r^{-2}$.

1.2.2 Models

1.2.2.1 MOND Gravitational forces have been measured on small scales in laboratories on Earth and tested in

⋆ E-mail: psteger@phys.ethz.ch

the solar system to yield consistent results, if calculated via the framework of general relativity. On larger scales, though, this has not been tested **(TODO: citation)**. MOND (Modified Newtonian Dynamics, Milgrom (1983)) assumes a more general form of gravitational interaction

$$\vec{F} = \mu(a/a_0)m\vec{a}, \quad (1)$$

$$\mu(x \gg 1) \sim 1, \quad (2)$$

$$\mu(x \ll 1) \sim x \quad (3)$$

which reduces to the known gravitational $F(r) \propto r^{-2}$ on small r. Instead of introducing a new particle type with exotic features to account for the missing mass one could tune α such that the interaction grows stronger with larger scales. The main problems of this approach are i) that no simple physical process seems to cause the expected behavior, and ii) that there remains the need for a yet unseen form of matter in clusters of galaxies. The bullet cluster (Clowe et al. 2006) shows a mismatch of the loci of gravitating mass and emission of a considerable fraction of gas in an ongoing merger and thus indicates that dark matter is some new particle rather than an effect from modified gravity.

1.2.2.2 Different velocity dispersions: Cold dark matter (CDM) is characterized by the fact that the proper motion of the particles is much smaller than the expansion rate of the Universe at freeze-out. CDM can collapse self-similarly on scales ranging from super-clusters down to the smallest galaxies. It decoupled from the temperature field in the early universe and started to form small structures, which build structures on larger scales subsequently.

Hot dark matter (HDM) consists of a particle type that is still freely streaming, as are the neutrinos. Its high velocities hinder structure formation below the mean free streaming path scale, which is the lower bound for any cores seen.

Additional models of Warm Dark Matter range in between these two extremes.

1.2.2.3 MACHOs and WIMPs: Massive astrophysical compact halo objects (MACHOs) such as brown dwarfs, planets and other small objects too faint to be seen by current telescopes contribute to the overall matter density in the Universe.

Model calculations **(TODO: citation)** showed that they do not sum up to the required amount of dark matter, supporting the existence of another type of particles (Weakly interacting massive particles, WIMPs).

This work implicitly assumes dark matter to be a particle given by the (lightest) superposition of supersymmetric particles (Jungman et al. 1996). **(TODO: really?)**

1.2.3 Possibilities for Detection

Experiments to detect dark matter directly are described e.g. in Schnee (2011). One generally differs between direct and indirect detection:

Direct detection searches for annihilation signals from high-energetic particles generated during interactions with material in detectors. The likelihood of interactions increase with the amount of detector material, and is generally low due to the small interaction crosssection predicted from cosmological constraints. Modern photon-detectors are sensitive and need shielding from cosmic rays and radioactive materials, which is generally accomplished by constructing them well below the surface of the Earth. Other direct detection experiments search for self-annihilation signals, i.e. particles generated from different channels of interactions with dark matter particles between themselves. These interactions are sensitive to the density squared, which raises the need to know where a high concentration of dark matter can be expected.

(TODO: Indirect detection experiments use)

To actually detect dark matter, one is interested in the expected density distribution of dark matter in galaxies, as Navarro et al. (1996) show.

Dynamics of stars in the solar neighborhood constrain the local dark matter density. For big distances, on the other hand, weak and strong lensing signals help to find the overall distribution of gravitating matter, and subtracting the visible matter yields the resulting dark matter profile.

1.3 Dwarf Galaxies

We adhere to the definition of dwarf galaxies as the smallest galaxies in the Universe with dynamical masses of $10^6 M_\odot - 10^8 M_\odot$ determined from visible components, while star masses range from $\sim 1000 M_\odot$ to $10^7 M_\odot$, and gas fractions of **(TODO: gas fractions)**.

An overview of the local group dwarf galaxies is given in Mateo (1998). Star formation histories of the dwarfs is covered e.g. in Skillman (2005) and Dolphin et al. (2005), kinematics in Walker et al. (2009) and Simon & Geha (2007), and their orbits in Lux et al. (2010).

Elliptical galaxies with luminosities below $10^9 L_\odot$ can be split in two families, one of which has much lower surface brightness and bigger radii than the other. This family is named dwarf spheroidals. They are so faint that they are only detected in the neighborhood of the Milky Way, with an estimated number count of 50-100 (Belokurov et al. 2007). They differ from other gravitationally bound systems in that they consist mostly of dark matter.

1.3.1 Observations

In galaxies with a mass as low as stated before, the luminosity is expected to be very low as well. This induces that only nearby dwarf galaxies can be observed with current observational instruments.

Observations showed some 10 classical dwarfs in the Milky Way halo **(TODO: citation)**. Recently, wide area surveys discovered more and more dwarfs, (Belokurov et al. 2007), (Belokurov et al. 2009), (Belokurov et al. 2010), totalling 25 in a 20% coverage of the sky (Koposov & Belokurov 2008). Following predictions of ΛCDM, there should be thousands of them, though **?**. This discrepancy is generally known as the "missing satellites problem", (Moore et al. 1999), (Klypin et al. 1999).

Moreover, observations give hints to the existence of a core in the central parts of rotationally supported dwarf galaxies. This is in contrast to theory predicting cuspy profiles for dark matter only profiles, (Moore 1994), (Flores & Primack 1994), (Moore et al. 1999).

It is not possible to disentangle the effects of the proposed mass profile from the anisotropic velocity distribution reliably.

The systems under study in e.g. de Blok et al. (2001) are gas-rich low surface brightness galaxies, with higher mass and more gas than our simulated dwarfs.

Looking at simulated small galaxies that are not necessarily rotationally supported, additional constraints as to which properties distinguish cores and cusps can be found. Baryons do play an non-neglectible role in dwarf dynamics, with proposed processes generating cores from cusps via i) non-adiabatic contraction ii) recurring baryonic in-/outflow (Read & Gilmore 2005), which could render the cusp-core problem pointless. This is in fact seen in simulations (Mashchenko et al. 2008), (Governato et al. 2009), which shows that the early assumption that baryon physics has only small influence were inaccurate (Navarro et al. 1996), (Gnedin & Zhao 2002).

? find that the scale of the outflows correlate with the size of the cored region.

1.4 Globular Clusters

Massive star clusters in the halo of the Milky Way - of which some 150 are detected by now. (Zinn 1985) and (De Angeli et al. 2005) show a mass in stars that is comparable to the dwarf spheroidals, typically 10^5 to $10^6 M_\odot$. The resemblance is going further as they have a similar age; they are mostly old, as old as the Universe itself. The big difference lies in the fact that they show little to no evidence for dark matter in them, whereas dynamics of dwarf spheroidals implies a mass fraction of 90% in dark matter. **(TODO: place, location)**

Why should stars form in environments with such a wide spread in density? Is there a connection between dwarf spheroidals and globular star clusters? Given there is one, how can it be determined qualitatively and quantitatively? It has been proposed **(TODO: citation)** that one is the evolved form of the other; or **(TODO: citation)** that they form in different environments.

By extracting basic properties that differ in between globular star clusters and dwarf spheroidals, one can try to answer that question. The temporal evolution of the defined substructures gives hints as to whether they represent different phases in an evolutionary path.

The density of globular clusters is such that in a typical patch of the LCDM Universe of size 1Mpc at $z = 10$ contains a few of them (Boley et al. 2009). **(TODO: really? not meant dwarf galaxies?)**

1.5 Simulations

The general paradigm behind simulations is as follows:

Simulations try to recover observations of todays structures and check theoretical models. This is done via setup of initial conditions with power spectrum similar to the the cosmic microwave background. In a first approximation, Gaussianity is assumed. For higher order terms, non-gaussianity is included via the correction term f_{NL}. **(TODO: state of the art, reason why not included)**

These initial conditions are power spectra for the modes of displacement in density and velocity, modeled on a grid of N^3 particles – and possibly further refinements – in a box. The box is assumed to repeat itself in each cartesian coordinate, effectively forming a hypertorus.

The simulation is then started and evolves the current state by calculating

- gravitational forces between particles
- hydrodynamical quantities, either for hydro particles or on a mesh
- the resulting changes for the next step

A review of how structure formation can be modeled by numerical means is found in Bagla (2005).

Collisional codes follow each of the particles directly, while collisionless simulations follow a smaller number of particles that are actually observed in the system. Collisional codes are used to follow systems in which close encounters play a significant role and need to be resolved, i.e. when the relaxation time is of order of the simulation timestep. In collisionless simulations one models a continuum distribution by sampling only a small number of particles. Dark matter as a pressureless fluid is often treated with this paradigma.

N-body simulations use a discrete sample of points in phase space to follow the evolution of the whole system. The track of a particle is determined by the gravitational force on it generated by the gravitational potential of all other particles. Any code that calculates this force and then follows the particle path and thereby integrates Poisson's equation is called a Poisson solver.

Particle-Particle-Particle-Mesh codes (PPPM) use direct summation of forces between all (star/dark matter) particles.

* **(TODO: PM)**

* Smoothed particle hydrodynamics (SPH) approaches the fluids by particles representing volume elements, and calculates the hydrodynamical forces from a discrete form of the Euler equations. Gadget is a prominent example of such a code.

Grid codes in contrast follow the gas dynamics in small patches and updates the hydro variables in the neighboring cells according to the flux through boundaries and volume changes. Meshes can take a diversity of geometries, depending on the physical system under consideration.

Adaptive mesh refinement (AMR) describes an advanced technology to follow the liquid more accurately: The mesh is refined in the vicinity of high overdensities or at discontinuities in the density, allowing for correct capture of accretion, shock waves, and other small features.

1.6 Overview this work

This work is organized as follos: After this introduction with an overview over the widespread field of dark matter research and methods of numerics in cosmology, we start by describing the simulations performed in section **??**, followed by a short explanation on the methods in section 2. We then focus on results: section 3 first concentrates on halo finding performance and general properties of the halos in a high resolution, hydrodynamical simulation, both for dark matter/stars and gas. This is compared with the properties found in a dark matter only simulation of the same intitial conditions, allowing to draw conclusions on the influence of baryons.

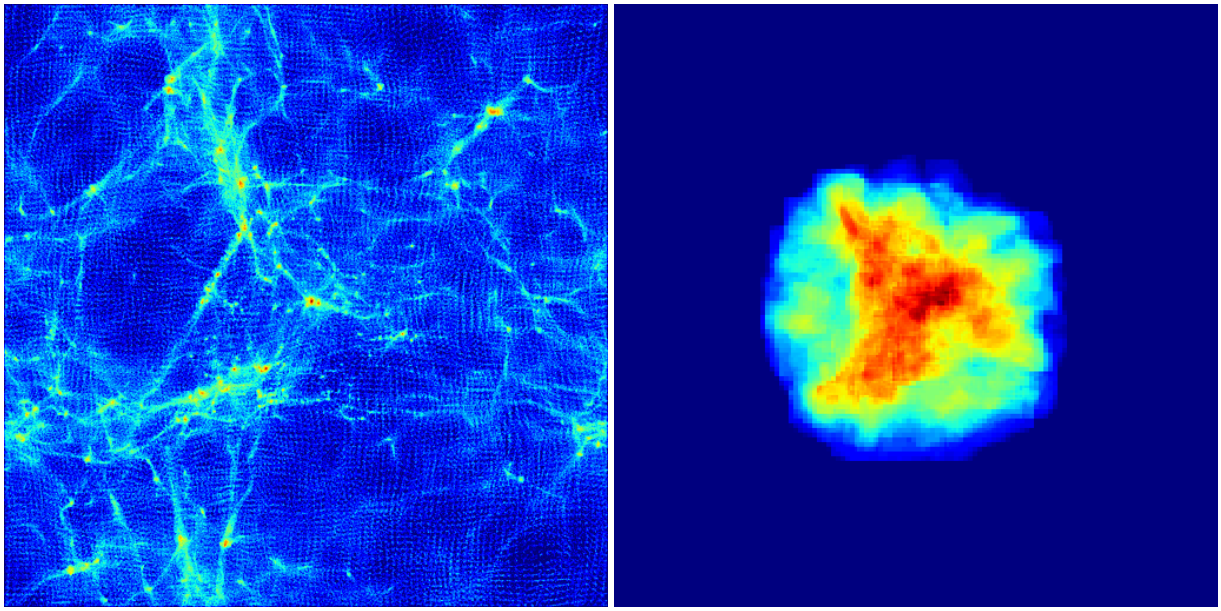

Figure 1. Visualization of one of the simulation box in the high resolution hydro run, with dark matter density in the left panel, and gas density encoded in a grid in the right box. The visible box size spans a range of 1 Mpc/h.

2 METHODS

2.1 The Simulations

Six simulations were run for this project. The main simulation was run with high resolution in a refined region, and including nonequilibrium chemistry to follow evolve reliable cooling rates down to temperatures below 10^4K. For comparative reasons the same resolution was used for a dark matter only simulation, and convergence was investigated by comparing that one to a lower dark matter only simulation. All simulations used the same cosmology, as follows.

2.1.1 Cosmological Parameters

The high resolution hydrodynamical simulation was run with WMAP-5 **(TODO: check valus in ICs)** concordance cosmology parameters, i.e. $\Omega_\Lambda = 0.742$, $\Omega_M = 0.258$, $\Omega_b = 0.045$, $h = 0.719$, $\sigma_8 = 1.0$.

2.1.2 Initial Conditions

Initial conditions were generated with Cosmics (Bertschinger 1995), for a box of 1Mpc/h boxlength, at $z = 1000$, with a low resolution boundary layer of 256^3 equivalent particles and an inner high resolution region of 256^3 particles, which again was refined by a factor 2 to match 245^3 particles in the second nested layer. The dark matter only, high resolution run was performed with 256^3 particles on the whole box. The mass resolution is thus set to **(TODO: check)** 120M$_\odot$. This corresponds to the average stellar mass to produce a supernova. By this procedure, we ensure that every supernova in our simulation corresponds to an actual star exploding.

2.1.3 Temporal coverage

The simulation is run from $z = 1000$ down to $z = 10$, with outputs on 100 equally spaced intervals, allowing to track specified structures back in time.

It has been shown in Boley et al. (2009) that in a typical volume of 1Mpc/h at $z \sim 10$ there should be a few dwarf spheroidal galaxies present. Thus the progenitors of todays dwarfs were generated before reionization. Its influence on the baryonic component will be considered in future work, e.g. via a windtunnel emulating the effects of ram-pressure stripping and shock front buildup during infall. **(TODO: so much/more detail?)**

2.1.4 Simulation physics

The same physics as in Boley et al. (2009) was used for the high resolution hydrodynamical simulation. This includes ram pressure, star formation, SN feedback, AGN. Ramses has beed used in a augmented version to follow nonequilibrium physics as well, namely the gas of e, HI, HII, HeI, HeII, HeIII, H^-, H_2, and H_2^+ (Abel et al. 1997). We do not include HD.

(TODO: network with reaction rate references)

2.2 Higher Resolution

We use significantly higher resolution than was previously performed (Boley et al. 2009), with non-equilibrium physics included.

The force resolution (Plummer's equivalent length) in the highest resolution mesh is **(TODO: update)** 4pc/h at $z = 10$, which sets a restriction on the determination of densities in the inner regions for the smallest halos. It is indicated as a vertical line in the graphs of radial profiles.

ID	description	box size [Mpc/h]	$z_{\rm start}$	$z_{\rm end}$	$n_{\rm DM}$	ε [pc/h]
hydro	full hydro physics high resolution	1	100	10	**(TODO: fill)**	4
dm low	dark matter only low resolution	1	100	10	**(TODO: fill)**	**(TODO: fill)**
dm high	dark matter only high resolution	1	100	10	**(TODO: fill)**	**(TODO: fill)**

Table 1. Properties of the simulations under study. ε gives the equivalent Plummer's width.

2.3 Definitions

2.3.1 Bound Structures

The virial radius r_{vir} is determined to be the distance from the densest point of a halo at which the mean enclosed density $\rho(r)$ is according Bryan & Norman (1998)

$$\rho(r) > \Delta(z)\rho_{crit,0} \quad (4)$$
$$\Delta(z) = 18\pi^2 + 82x - 39x^2 \quad (5)$$
$$x = \Omega(z) - 1 \quad (6)$$
$$\Omega(z) = \Omega_0(1+z^3)/E(z) \quad (7)$$
$$E(z) = \sqrt{\Omega_0(1+z^3) + \Omega_R(1+z)^2 + \Omega_\Lambda} \quad (8)$$

2.3.2 Radial Profile

The radial density profile $\rho(r)$ is determined from logarithmically spaced shells around the detected centers.

$$r_i = \textbf{(TODO: fill)} \quad (9)$$

2.3.3 Halo Finding

The simulation outcome by itself shows only properties of individual dark matter particles, and additionally a mesh for the hydrodynamical constituents. One is interested in bound substructures, which have to be found first by a halo finding technique.

2.3.3.1 FOF: The friend-of-friends algorithm as e.g. described in Press & Davis (1982) starts with a particle and searches for its nearest neighbor, out to a predefined radius. After doing this iteratively, all particles connected by such a chain are considered to lie within the same halo. This procedure works well for isolated halos only; two nearby halos connected by a filament could be detected as one structure only. Recent findings (**?**) **(TODO: include in bibliography)** show that the overdensity inside the virial radius is typically of order 80 instead of the generally expected 180. **(TODO: other flavors, state of the art)**

2.3.3.2 HOP: HOP from the RAMSES toolkit starts off by computing the density around each particle with an adaptive kernel, then hops to the neighbor particle at highest density, and assigning all particles ending at the same point to the same structure. Breaking up due to local density maxima is overcome by merging two groups if the density of the boundary layer between them lies above a given threshold.

2.3.3.3 Watershed: The watershed algorithm **?** starts from the density maxima as leaves of the halo/subhalo tree. Stepping further out, all material in the same potential pot is assigned to the respective maxima. As soon as a neighbor maximum is encountered, both halos form an additional leave in the tree.

2.3.3.4 SOD: The spherical overdensity algorithm as introduced by Lacey & Cole (1994) grows a sphere around particles at density minima and stops if the mean density falls below a threshold. This procedure is repeated with the remaining particles until no structure with a minimum number of particles is found anymore. It does not handle correctly the cases of mergers, yielding a halo position in the middle of both merging halos.

Here the AHFSTEP algorithm of the simulation code AMIGA **(TODO: citation)** is used. It showed superior capabilities with mock halos and subhalos **(TODO: citation)**.

The prospective halo centers can be defined in several ways: by the position of the center of mass, the center of the potential or the density maximum. Visually best agreement with dark matter density projection was found for the position of maximal density.

An additional iterative procedure excludes all particles which are kinematically unbound: if the kinetic and internal energy (for hydro particles) exceed the potential energy, the particle is removed, the potential recalculated and further unbound particles excluded.

Additional displacements with respect to the densest point were corrected with an additional shrinking sphere algorithm: It starts from the center of mass of all particles in a sphere of radius $r_{\rm vir}$, then rescales the radius to $r_{i+1} = f \cdot r_i$, $f \leqslant 1$, and considers only particles inside the smaller sphere to find the center of mass in the next step, until the positions converge to $(\Delta x_{i\to i+1} - \Delta x_{i-1\to i})/\Delta x_{i\to i-1} < \varepsilon$. Similar restrictions on the convergence of COM velocity were not considered. The two parameters f and ρ are not restricted by a physical argument and thus have been chosen such that for the majority of massive halos convergence was reached in < 100 steps, with displacements $< 0.1 r_{\rm vir}$. **(TODO: redo)**

2.4 Halo Selection

We are interested in the inner density profile of dwarf spheroidals, therefore, only halos with virial mass above $10^7 M_\odot/h$ and no host halo are considered further. Their main properties are listed in table 2.

2.5 Relaxation Radius

The relaxation radius was determined according to definitions and methods described in Read (2009). N is the total particle number enclosed in a sphere of radius r around the center with a mass of $M(< r)$, $b_{\rm max}$ and $b_{\rm min}$ are maximal

Simulation	ID	$M_{\rm vir}/h^{-1}{\rm M}_\odot$	$R_{\rm vir}/h^{-1}{\rm pc}$	x	y	z	f_{DM}	f_{gas}	f_{stars}
hydro	1	$4.070 \cdot 10^7$	$8.52 \cdot 10^3$	0.5095	0.5064	0.4941			
hydro	2	$1.522 \cdot 10^7$	$6.14 \cdot 10^3$	0.5214	0.5040	0.4801			
hydro	3	$1.410 \cdot 10^7$	$5.98 \cdot 10^3$	0.3987	0.6329	0.6409			
hydro	4	$1.336 \cdot 10^7$	$5.88 \cdot 10^3$	0.3886	0.6167	0.6376			
hydro	5	$1.108 \cdot 10^7$	$5.52 \cdot 10^3$	0.4338	0.3954	0.4415			
dm	1	$5.579 \cdot 10^7$	$9.46 \cdot 10^3$	0.3629	0.3630	0.3579	1.0	0.0	0.0
dm	2	$4.205 \cdot 10^7$	$8.61 \cdot 10^3$	0.2648	0.0773	0.4323	1.0	0.0	0.0
dm	3	$3.036 \cdot 10^7$	$7.73 \cdot 10^3$	0.2844	0.4540	0.4588	1.0	0.0	0.0
dm	4	$2.822 \cdot 10^7$	$7.54 \cdot 10^3$	0.1983	0.6295	0.3276	1.0	0.0	0.0
dm	5	$1.999 \cdot 10^7$	$6.72 \cdot 10^3$	0.2574	0.5456	0.5674	1.0	0.0	0.0

Table 2. Properties of the selected halos. $M_{\rm vir}$ and $R_{\rm vir}$ are the virial mass and radius of the halos, f_i gives the fraction of mass in component i.

and minimal impact parameter, which are set to virial radius and gravitational force softening length in a first step.

$$t_{\rm relax} = n_{\rm cross} t_{\rm cross} \sim \frac{N}{16\pi \ln \Lambda} t_{\rm orb} \quad (10)$$

$$t_{\rm orb} = 2\pi b_{\rm max} \sqrt{\frac{b_{\rm max}}{GM(<r)}} \quad (11)$$

$$\ln \Lambda = \ln \frac{b_{\rm max}}{b_{\rm min}} \quad (12)$$

$$t_{\rm relax}(r) = \frac{N b_{\rm max}^{3/2}}{8\sqrt{GM(<r)}\ln(b_{\rm max}/b_{\rm min})} \quad (13)$$

$$t_{\rm sim} = t_{\rm relax}(r_{\rm relax}) \quad (14)$$

The last equation is solved for $r_{\rm relax}$ by a basic root finding algorithm. All quantities determined from particles inside $r_{\rm relax}$ are expected to be widely independent of the properties of the surrounding halo, as any memory was erased in numerous encounters. The relaxation radius can be defined in several ways for simulated systems, with better matches when $b_{\rm max} = r$, allowing the Coulomb logarithm $\ln \Lambda$ to change slowly with radius.

3 RESULTS

3.1 DM density profile

Dark matter density profiles are shown in fig. **??** for the most massive halo in each simulation at $z = 10$. The vertical blue line indicates the force softening length on the most refined grid in the hydrodynamical run. All values at smaller radii are not to be trusted.

Fig. 3 shows the profiles for the halos DM 1-5.

Fig. 4 shows both dark matter and star density profiles for HYDRO 1 and HYDRO 5. **(TODO: Adiabatic contraction)**

3.2 Halo finding

It is important to center the halos correctly on the most dense point, as a little offset implicates an overdensity at the radius of offset, thus turning a cusp into a broader core. Fig. 5 shows positions and virial radii detected with two of the above mentioned methods, spherical overdensity (SOD, pink circles) and AHF (red crosses).

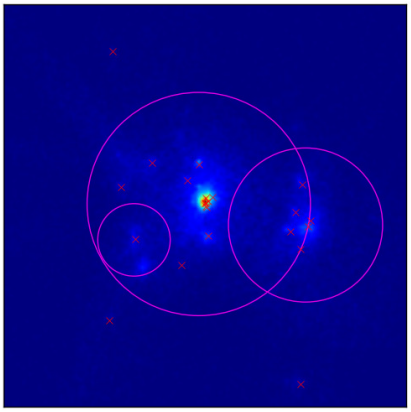

Figure 5. Positions of the halos detected by SOD (blue circle) and AHF (red crosses) on top of dark matter density. The radii of the circles corresponds to the value of r_{vir} as detected by SOD.

Fig. 6 and **??** give an overview of HYDRO 1 and HYDRO 5 as the most massive and least massive halo considered. Projections along the three axes x, y, z of dark matter density, star density and AMR grid (proportional to gas density) are shown.

Additional centering with the shrinking sphere algorithm for values of $f = 0.1$ and $\varepsilon = 0.01$ resulted in displacements as shown in fig. **??**. This method relies on a sensible choice of both of these values, which need to be set for each halo separately. There is no considerable change for the massive halos, and only the centers of small subhalos get affected.

3.3 Stars

Fig. **??** shows a projection of all stars in HYDRO 1, plotted on the overall density distribution. The size of the stars is proportional to their metallicity. Assuming that groups of stars forming at roughly the same time in the same region should show approximately the same metallicity, one draws

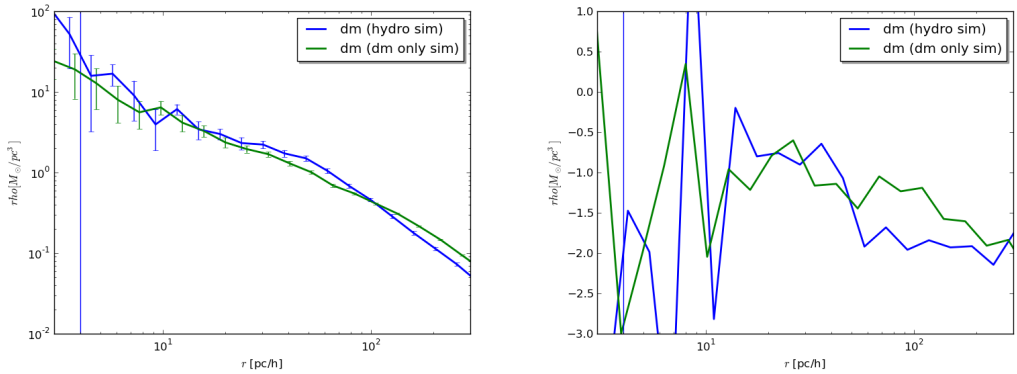

Figure 2. Dark matter density profiles for the most massive halo in both runs.

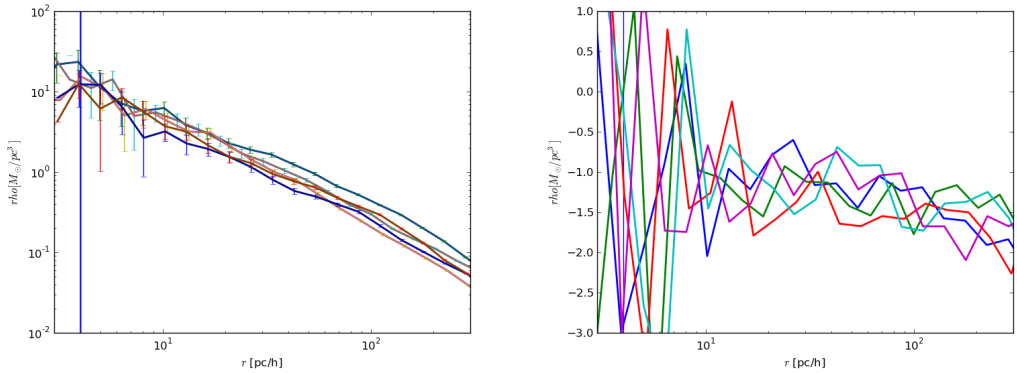

Figure 3. Dark matter density profile of the five most massive halos

the conclusion that they first formed outside the halo before being accreted.

4 SUMMARY AND DISCUSSION

4.1 Impacts on Formation History

4.2 Local DM Density

The local dark matter density Garbari et al. (2010) is a superposition of dark matter from the disc and the halo of the Milky Way. Simulations of dwarf galaxies as studied above falling through the disc could help to constrain the evolution of the vertical density profile.

ACKNOWLEDGEMENTS

I warmly thank J. Read for many helpful discussions and the pleasant environment. A. Hobbs broadened my horizon on numerical astrophysics. A precursor hydrodynamic simulation and the underlying implementation of NEC cooling was performed by A. Boley, who gave useful technical hints as well. S. Garbari provided a prototype algorithm for the correction of the prospective halo centers.

5 APPENDIX: NUMERICAL ROBUSTNESS, CONVERGENCE

The low resolution simulation was used to check convergence of the high resolution dark matter only simulation.

REFERENCES

Abel T., Anninos P., Zhang Y., Norman M. L., 1997, Nature, 2, 181
Bagla J. S., 2005, Current Science, 88, 1088
Belokurov V., Walker M. G., Evans N. W., Gilmore G., Irwin M. J., Just D., Koposov S., Mateo M., Olszewski E., Watkins L., Wyrzykowski L., 2010, ApJ, 712, L103
Belokurov V., Walker M. G., Evans N. W., Gilmore G., Irwin M. J., Mateo M., Mayer L., Olszewski E., Bechtold J., Pickering T., 2009, MNRAS, 397, 1748
Belokurov V., Zucker D. B., Evans N. W., Kleyna J. T., Koposov S., Hodgkin S. T., Irwin M. J., Gilmore G., Wilkinson M. I., Fellhauer M., Bramich D. M., 2007, ApJ, 654, 897
Bertschinger E., 1995, ArXiv Astrophysics e-prints
Binney J., Tremaine S., 2008, Galactic Dynamics: Second Edition. Princeton University Press
Boley A. C., Lake G., Read J., Teyssier R., 2009, ApJ, 706, L192

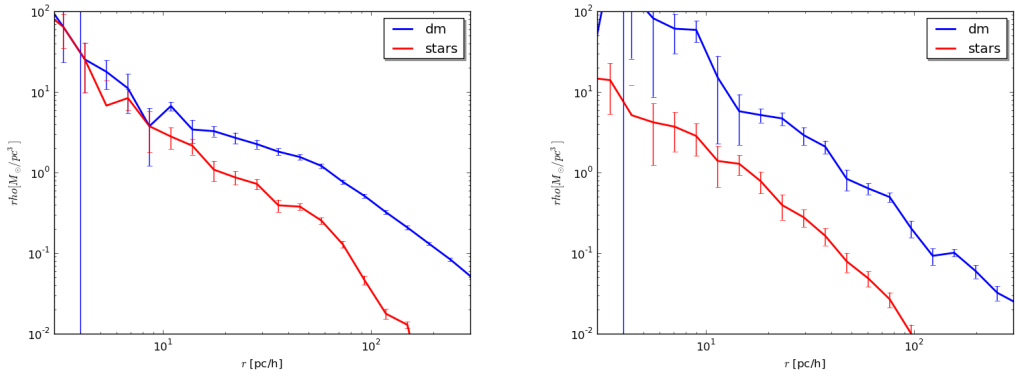

Figure 4. Density profile of dark matter and star particles in (HYDRO 1) and (HYDRO 5)

Bryan G. L., Norman M. L., 1998, ApJ, 495, 80
Clowe D., Bradač M., Gonzalez A. H., Markevitch M., Randall S. W., Jones C., Zaritsky D., 2006, ApJ, 648, L109
De Angeli F., Piotto G., Cassisi S., Busso G., Recio-Blanco A., Salaris M., Aparicio A., Rosenberg A., 2005, AJ, 130, 116
de Blok W. J. G., McGaugh S. S., Rubin V. C., 2001, AJ, 122, 2396
Dolphin A. E., Weisz D. R., Skillman E. D., Holtzman J. A., 2005, ArXiv Astrophysics e-prints
Flores R. A., Primack J. R., 1994, ApJ, 427, L1
Garbari S., Lake G., Read J., 2010, in V. P. Debattista & C. C. Popescu ed., American Institute of Physics Conference Series Vol. 1240 of American Institute of Physics Conference Series, Measuring the Local Dark Matter Density. pp 411–412
Gnedin O. Y., Zhao H., 2002, MNRAS, 333, 299
Governato F., Brook C., Mayer L., Brooks A., Rhee G., Wadsley J., Jonsson P., Willman B., Stinson G., Quinn T., Madau P., 2009, ArXiv e-prints
Jungman G., Kamionkowski M., Griest K., 1996, Phys. Rep., 267, 195
Klypin A., Kravtsov A. V., Valenzuela O., Prada F., 1999, ApJ, 522, 82
Komatsu E., Dunkley J., Nolta M. R., Bennett C. L., Gold B., Hinshaw G., Jarosik N., Larson D., Limon M., Page L., Spergel D. N., Halpern M., Hill R. S., Kogut A., Meyer S. S., Tucker G. S., Weiland J. L., Wollack E., Wright E. L., 2009, ApJS, 180, 330
Koposov S., Belokurov V., 2008, Observational Constraints on the "Missing Satellite" Problem from SDSS. pp 195–+
Lacey C., Cole S., 1994, MNRAS, 271, 676
Lux H., Read J. I., Lake G., 2010, MNRAS, 406, 2312
Mashchenko S., Wadsley J., Couchman H. M. P., 2008, Science, 319, 174
Mateo M. L., 1998, ARA&A, 36, 435
Milgrom M., 1983, ApJ, 270, 365
Moore B., 1994, Nature, 370, 629
Moore B., Ghigna S., Governato F., Lake G., Quinn T., Stadel J., Tozzi P., 1999, ApJ, 524, L19
Moore B., Quinn T., Governato F., Stadel J., Lake G., 1999, MNRAS, 310, 1147
Navarro J. F., Frenk C. S., White S. D. M., 1996, ApJ, 462, 563
Padmanabhan T., 1993, Structure Formation in the Universe
Peacock J. A., 1999, Cosmological Physics
Press W. H., Davis M., 1982, ApJ, 259, 449
Read J. I., 2009, Astrophysical Dynamics. University Leicester, UK
Read J. I., Gilmore G., 2005, MNRAS, 356, 107
Schnee R. W., 2011, ArXiv e-prints
Simon J. D., Geha M., 2007, ApJ, 670, 313
Skillman E. D., 2005, Nature, 49, 453
Walker M. G., Mateo M., Olszewski E. W., Peñarrubia J., Wyn Evans N., Gilmore G., 2009, ApJ, 704, 1274
Weinberg S., 2008, Cosmology. Oxford University Press
Zinn R., 1985, ApJ, 293, 424
Zwicky F., 1933, Helvetica Physica Acta, 6, 110

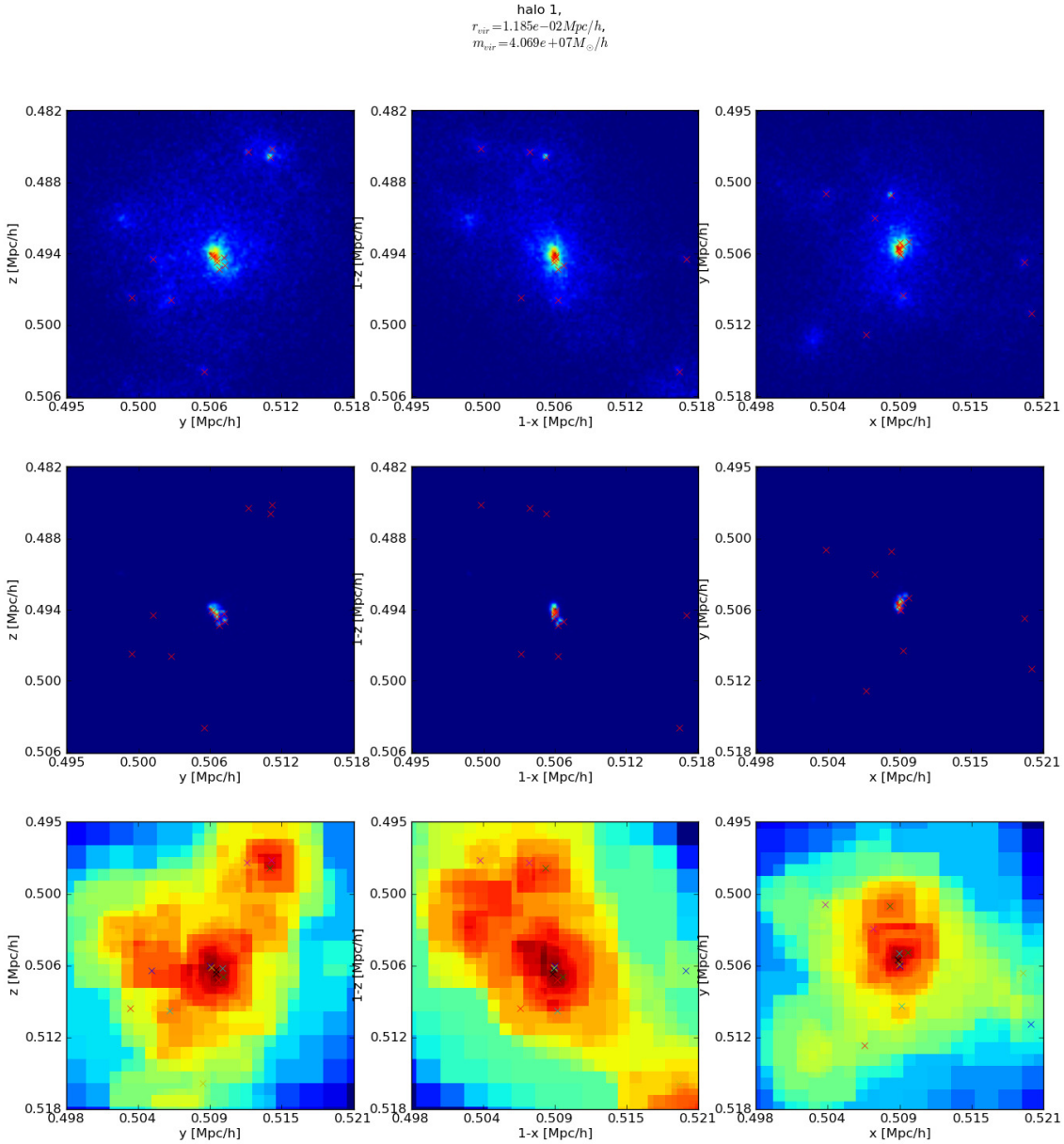

Figure 6. Projections of dark matter density (top row), star density (middle row) and AMR grid (bottom row) along all three axes for halo HYDRO 1.

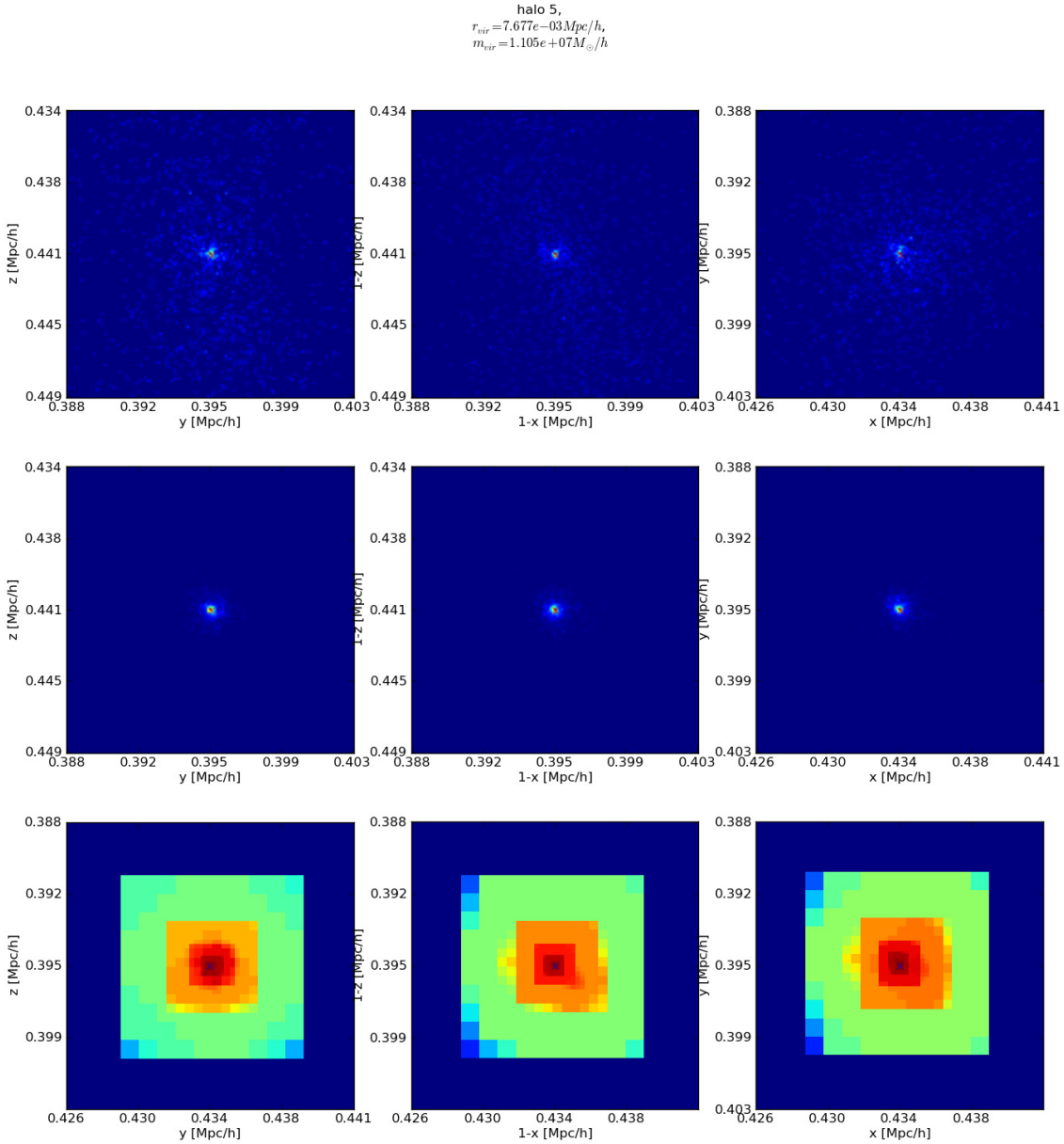

Figure 7. Projections of dark matter density (top row), star density (middle row) and AMR grid (bottom row) along all three axes for halo HYDRO 5.